29 Jun 2018

Inelastic Response Evaluation of Precast Composite Columns under Seismic Loads

Mohanad M. Abdulazeez

Mohamed ElGawady
Missouri University of Science and Technology, elgawadym@mst.edu

Recommended Citation

M. M. Abdulazeez and M. ElGawady, "Inelastic Response Evaluation of Precast Composite Columns under Seismic Loads," *Proceedings of the 11th U.S. National Conference on Earthquake Engineering (2018, Los Angeles, CA)*, pp. 1729-1739, Earthquake Engineering Research Institute, Jun 2018.

Eleventh U.S. National Conference on Earthquake Engineering
Integrating Science, Engineering & Policy
June 25-29, 2018
Los Angeles, California

INELASTIC RESPONSE EVALUATION OF PRECAST COMPOSITE COLUMNS UNDER SEISMIC LOADS

Mohanad M. Abdulazeez[1]; and Mohamed A. ElGawady[2§], PhD, M. ASCE

ABSTRACT

This paper presents a non-linear finite element analysis of large-scale hollow-core fiber-reinforced polymer-concrete-thin walled steel (HC-FCS) precast columns under reversed cyclic loading. The HC-FCS columns provide an economical and efficient alternative to conventional concrete bridge columns. The precast HC-FCS column consists of a concrete shell sandwiched between an outer fiber-reinforced polymer (FRP) tube and an inner thin-walled steel tube. The steel tube diameter-to thickness (D_i/t_s) ratio was 254. The proposed FEA model was developed using LS_DYNA multipurpose software and was verified by experimental results performed in this study. The FE model was used to investigate some important phenomena such as thin-walled steel tube cyclic local buckling and to determine where and when steel tube yielding and damage initiation occurs. The comparison and analysis of the proposed model to predict local damages, failure patterns, and hysteretic curves were in reasonable accuracy with the experimental outcomes.

[1] Graduate Research Assistance and PhD student, Dept. of Civil, Architectural, and Environmental Engineering, Missouri University of Science and Technology, Rolla, MO. 65401; mma548@mst.edu
[2] Benavides Associate Professor, Dept. of Civil, Architectural, and Environmental Engineering, Missouri University of Science and Technology, Rolla, MO. 65401; elgawadym@mst.edu
[§]Corresponding author

Inelastic response evaluation of precast composite columns under seismic loads

Mohanad M. Abdulazeez[1]; and Mohamed A. ElGawady[2§], PhD, M. ASCE

ABSTRACT

This paper presents a non-linear finite element analysis of large-scale hollow-core fiber-reinforced polymer-concrete-thin walled steel (HC-FCS) precast columns under reversed cyclic loading. The HC-FCS columns provide an economical and efficient alternative to conventional concrete bridge columns. The precast HC-FCS column consists of a concrete shell sandwiched between an outer fiber-reinforced polymer (FRP) tube and an inner thin-walled steel tube. The steel tube diameter-to thickness (D_i/t_s) ratio was 254. The proposed FEA model was developed using LS_DYNA multipurpose software and was verified by experimental results performed in this study. The FE model was used to investigate some important phenomena such as thin-walled steel tube cyclic local buckling and to determine where and when steel tube yielding and damage initiation occurs. The comparison and analysis of the proposed model to predict local damages, failure patterns, and hysteretic curves were in reasonable accuracy with the experimental outcomes.

Introduction

It's estimated that Americans spend 14.5 million hours per day in traffic. 10 to 15% of that congestion is caused by work zones. Even when work zones occur during off-peak times, they increase traffic congestion [1, 2]. Reducing the amount of time it takes to construct roads and bridges from months to days or even hours is highly desirable. Accelerated bridge construction (ABC) represents a paradigm which minimizes the mobility impact of on-site construction. It uses innovative planning methods, materials, and designs in a safe and cost effective manner resulting in reduces on-site construction time is reduced when building new bridges or rehabilitating and replacing existing ones.

ABC includes such elements as prefabricated modular units that are built off-site in a controlled environment and then transferred to the construction area for rapid installation. ABC reduces traffic disruptions and life-cycle costs and improves construction quality and safety, resulting in more sustainable development [3]. One technique to accelerate bridge construction is to use precast bridge columns with excellent seismic performance.

[1] Graduate Research Assistance and PhD student, Dept. of Civil, Architectural, and Environmental Engineering, Missouri University of Science and Technology, Rolla, MO. 65401; mma548@mst.edu

[2] Benavides Associate Professor, Dept. of Civil, Architectural, and Environmental Engineering, Missouri University of Science and Technology, Rolla, MO. 65401; elgawadym@mst.edu

§Corresponding author

A good candidate for precast columns is the concrete-filled tube, which consists of a hollow tube made out of steel or fiber-reinforced polymer filled with concrete. Another candidate for precast columns is the hollow-core steel-concrete-steel (HC-SCS) column consisting of two generally concentric tubes with concrete shell between them ([Fig. 1)[4-12]. The inner tube is empty, i.e., unfilled with concrete to reduce the weight of the column. HC-SCS columns can also be cast-in-place, with the outer and inner tubes acting as stay-in-place formwork.
The concrete infill is confined by both tubes, resulting in high concrete confinement and column ductility [11]. All of the mentioned research showed the superior seismic and axial capacity of HC-SCS columns.

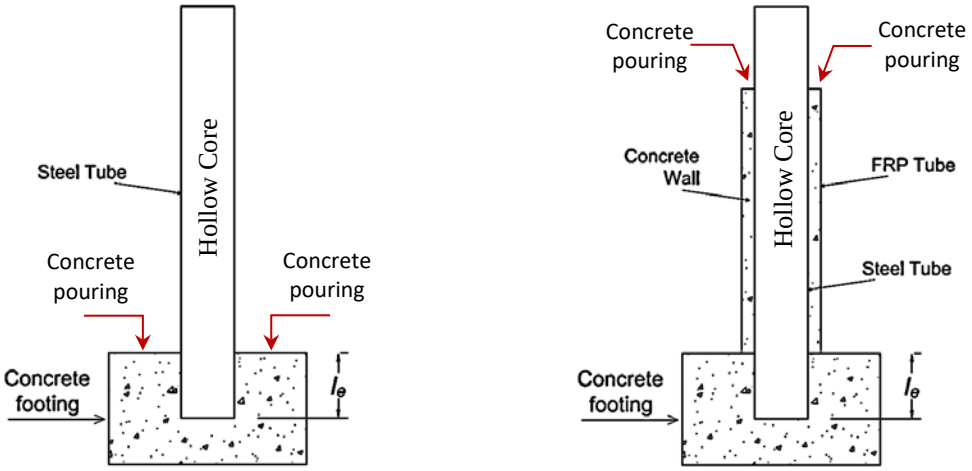

(a) (b)

Figure 1. General arrangement of the construction of the HC-FCS column (a) inserting the steel tube and casting the footing, (b) installing the FRP tube and pouring the concrete shell.

This paper presents a 3D FE model of HC-FCS columns having inner thin-walled steel tube that is capable of capturing the inelastic response, damage criteria, and local deformations under axial and quasi-static cyclic loads. The accuracy of the proposed FE model is examined by comparison with the results of the experimental test.

Experimental program

In this study, a 0.4-scale HC-FCS column, F4-24-E3-0.5-4, was tested under constant axial load and lateral cyclic load. The F4-24-E3(0.5)4 column had a circular cross section with an outer diameter (D_f) of 24 inches and a clear height of 80 inches. The lateral load was applied at a height of 95 inches with a shear span-to-depth ratio of approximately 4.0. The column consisted of an outer glass fiber filament-wound (GFRP) tube with a thickness of 0.38 inches. The inner steel tube had an outer diameter of 16 inches and a thickness of 0.063 inches corresponding to an inner-diameter-to-thickness (D_i/t_s) ratio of 254. The steel tube was manufactured in the High-Bay Structural Engineering Research Laboratory at Missouri University of Science and Technology by performing a seam-welding (full-penetration groove weld according to AWS 2000) for a 0.063-inch steel sheet cut and rolled to the required dimensions (length x circumference) prior to the

welding. The columns' label used in the current experimental work consisted of four segments. The first segment is a letter "F" in reference to flexural testing, followed by the column's height-to-outer diameter ratio (H/D_f). The second segment refers to the column's outer diameter (D_f) in inches. The third segment refers to the GFRP matrix using "E" for epoxy base matrices; this is followed by the GFRP thickness in 1/8 inches, steel thickness in 1/8 inches, and concrete shell thickness in inches.The steel tube of the column was embedded into the footing while the FRP tube truncated at the face of the footing without any embedment. The embedment depth, l_e, was determined using Eq. 1 [13]

$$\frac{D_i t_s F_u}{\left(l_e{}^2\right)} \leq 3.3\sqrt{f'_{c,FT}} \quad (1)$$

where D_i is the steel tube's outer diameter (being 16 inches), t_s is the steel tube thickness (being 0.063 inches), F_u is the ultimate stress of steel tube (being 56,000 psi), and $f'_{c,FT}$ is the unconfined cylindrical compressive strength of the concrete footing (being 5,500 psi). Using these values, an embedded length of 20 inches was deduced. Therefore, during the experimental work, l_e of 20 inches corresponding to 1.25 D_i (D_i being the inner diameter of the steel tube) was used to achieve the full embedment of the HC-FCS column.

The concrete footing that was used in this study had a length x width x depth of 60 inches x 48 inches x 34 inches with bottom reinforcements of 7-#7, top reinforcements of 6-#7, and shear reinforcement of #4 at 2.5 inches. The steel cage of the footing was installed into the formwork.

The construction steps were as follows: 1) preparing and installing the reinforcement cages of the footings; 2) installing the steel tube into the footing cage with an embedded length of 20 inches; 3) pouring the concrete of the footing; 4) installing the GFRP tube and pouring the concrete of the concrete shell with a thickness of 4 inches; 5) installing the reinforcement cage of the column head with dimensions of 30 inches long x 30 inches wide x 32 inches deep followed by concrete pouring.

The used GFRP tube, based on the manufacturer's datasheet, had an elastic modulus of 677 ksi, hoop elastic modulus of 3,020 ksi, axial ultimate stress of 12,150 psi, and hoop rupture stress of 40,150 psi. The inner steel tube had a yield stress of 56,000 psi, ultimate stress of 63,000 psi, yielded strain of 2.35%, and an ultimate strain of 6.7%. The steel rebar had a yield stress of 60,000 (psi), ultimate stress of 90,000 (psi), and ultimate strain of 0.08. The rebar properties are based on the manufacturer's data sheet while the steel tube properties were determined through tensile steel-coupon testing according to ASTM A1067. Pea gravel with a maximum aggregate size of 3/8 inch was used for the concrete mixtures. The unconfined concrete strengths ($f'c$) for F4-24-E3(0.5)4 at 28 days and at the day of the test were 6,305 (psi) and 6,610 (psi) for the column, while 5,960 (psi) and 6,445 (psi) were obtained for the footing of the same age, respectively.

Loading protocol and test setup

A constant axial load, P, of 110 kips, corresponding to 5% of the axial load capacity of the equivalent RC-column, P_o, with the same diameter and 1% longitudinal reinforcement ratio, was applied to the column using six external prestressing strands (Fig. 2). The P_o was calculated using Eq. 2 (AASHTO-LRFD 2012):

$$P_o = A_s F_y + 0.85(A_c - A_s)f'c \quad (2)$$

where A_s = the cross-sectional area of the longitudinal steel reinforcements, A_c = the cross-sectional area of the concrete column, and F_y = the yield stress of the longitudinal steel

reinforcements. The prestressing strands were supported by a rigid steel beam atop the column and the column's footing. The prestressing force was applied using two servo-controlled jacks that kept the prestressing force constant during the test.

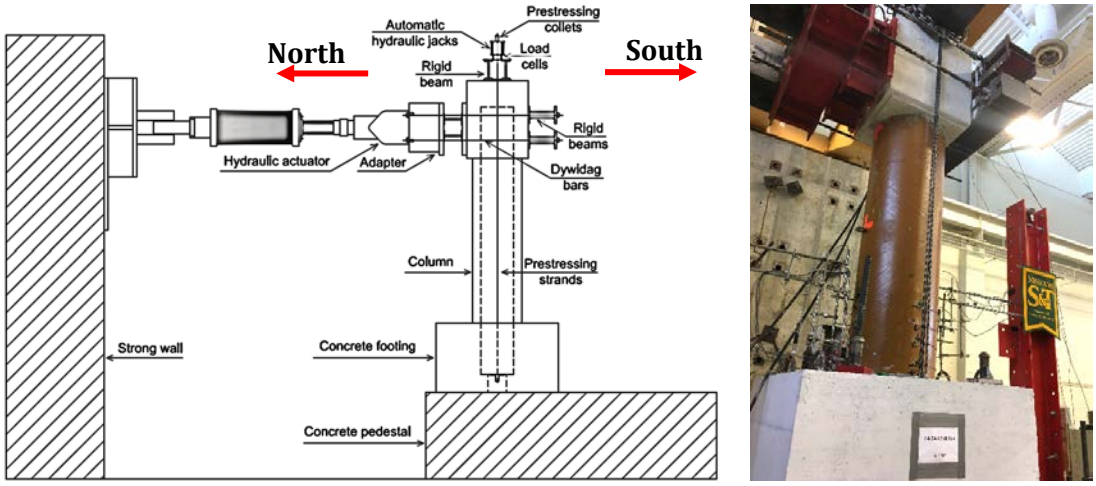

(a) (b)

Figure 2. (a) Layout of the test setup, (b) The F4-24-E3(0.5)4 column prior to the testing.

FE Modeling of HC-FCS columns having thin-walled steel tube

Sensitivity analyses were conducted to determine the optimum sizes of the different element. The final model had 13,319 elements and 16,329 nodes [Fig. 3 (a), (b) and (c)]. Surface-to-surface contact elements were used to simulate the interface between the concrete shell and outer FRP tube as well as the concrete shell and inner steel tube. Node-to-surface contact elements were used between the steel tube ends at the top with the loading stub and at the bottom inside the footing. Likewise, this type was used to simulate the contact between the FRP tube to the footing with a coefficient of friction of 0.6 (Abdelkarim and ElGawady 2014).

Concrete

A concrete damage plasticity (CDP) model built in LS_DYNA material model, the K&C concrete model (Mat_72R3), was implemented to simulate the seismic behavior of concrete [14-16]. CDP is an isotropic plasticity model that is similar to the Drucker-Prager model in term of the concrete compressive behavior. The K&C model proved to be highly accurate for simulating the concrete wall shell under triaxial stress state due to the confining effect. This model considers three shear failure surfaces: (1) yield, (2) maximum, and (3) residual with automatically generated parameters given the unconfined concrete compressive strength f_c' [17]. This model is implemented into the LS_DYNA software by using an eight-node solid element with reduced integration for the footing, concrete wall, and loading stub, as in Fig.3 (d) and (f).

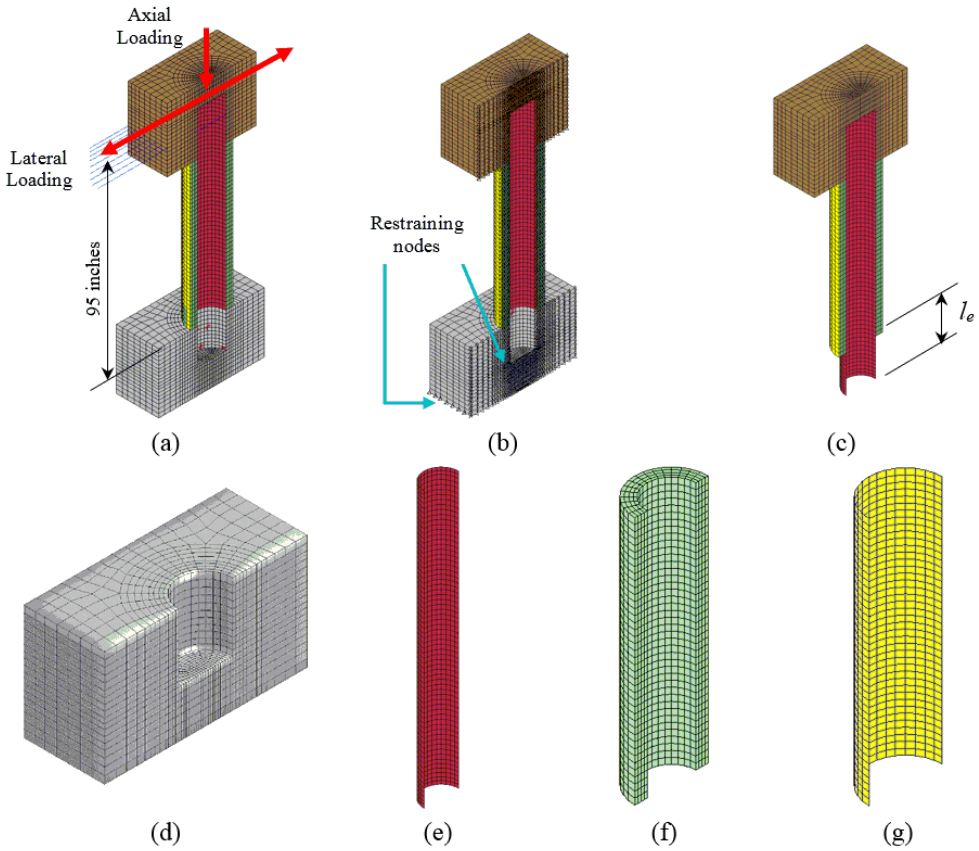

Figure 3. FE modeling (a) F4-24-E3(0.5)4, (b) the column restraining nodes, (c) steel tube embedded length, (d) concrete footing, (e) steel tube, (f) concrete wall, (g) FRP tube.

Thin-walled steel tube

A cyclic damage plasticity model MAT_DAMAGE_3 was used to model the steel tube behavior under reversed cyclic loads. For the thin-walled steel tube, it is important to consider the effect of the local buckling on the hysteretic behavior accompanied by the cyclic material plasticity. Therefore, this material model was selected which combined isotropic/kinematic plasticity and damaged evaluation for modeling low cycle fatigue and failure of the steel tube [18-20]. Displacement damage evolution (DDE) type was implemented to define the damage initiation as a function of the plastic displacement after damage initiation. The steel material was defined based on the average true stress-strain relationship curve depicted in Fig. 4(a) from the obtained tube coupon test results, as in Fig. 4(b) according to ASTM E8/E8M - 16a (note that the elastic modulus was 30,500 ksi). The inner steel tubes were simulated using Belytsehko-Tsay four-node shell elements with six degrees of freedom per node as in Fig. 3(e). This type of shell elements takes into account the geometrical nonlinearity to express accurately the local buckling behavior.

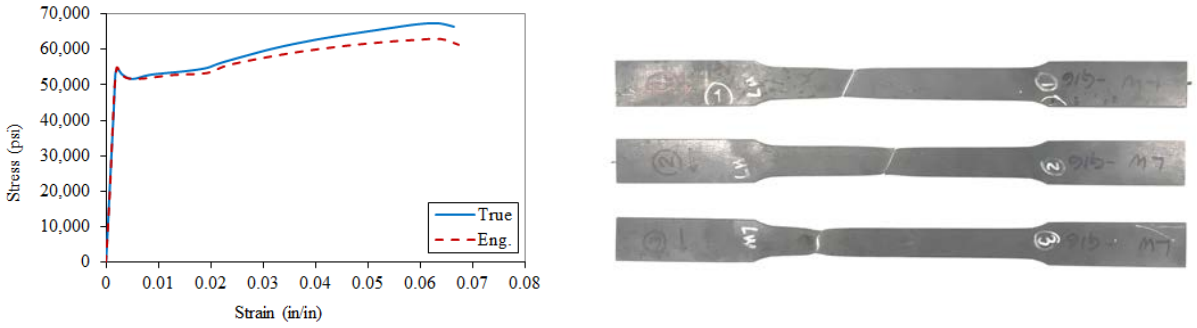

(a) (b)

Figure 4. Uniaxial stress-strain curve (a) stress-strain relationship curve, (b) steel tube coupons

FRP tube

An orthotropic elastic material denoted as 002-ORTHOTROPIC_ELASTIC was used to simulate the GFRP tube. The GFRP has an elastic moduli and ultimate rupture stress in the hoop direction of 3,020 ksi and 40.15 ksi, respectively. The major Poisson's ratio was 0.25. A failure criterion for the GFRP elements was implemented in LS_DYNA by defining an ultimate GFRP strain, using 000-ADD_EROSION, of 1.3%. The outer FRP tube was simulated using Belytsehko-Tsay four-node shell elements with six degrees of freedom per node as in Fig. 3(g).

Boundary conditions and loading

The tested column was symmetric; hence, only one half of the column was modeled in LS_DYNA, as in Fig. 3. The middle of the column was used as a plane of symmetry. The column was loaded using half of the axial compressive load applied to the top of the loading stub due to the symmetry. Then, the column was loaded laterally with a linear ramp up displacement at the middle nodes of the head side at a height of 95 inches. This was done by modeling the actuators as a beam elements with the end and middle boundary load applying conditions.

Results and discussion

Fig. 5 compares the cyclic response of the experimental and FE results. The lateral drift (δ) was calculated by dividing the lateral displacement measured from the actuators' displacement transducers by the shear span of 95 inches. The moment (M) at the base of the column was obtained by multiplying the force measured by the actuators' load cells by the column's height of 95 inches. The maximum moment capacity and the lateral drift were 237 kip.ft and 11.4%. A 3D finite element model was developed using LS_DYNA software and validated using the measured response and observed damage of the test results. The FE model predicted 93% of the experimental ultimate moment capacity and 97% of the experimental ultimate displacement capacity of the tested column as shown in Fig. 5.

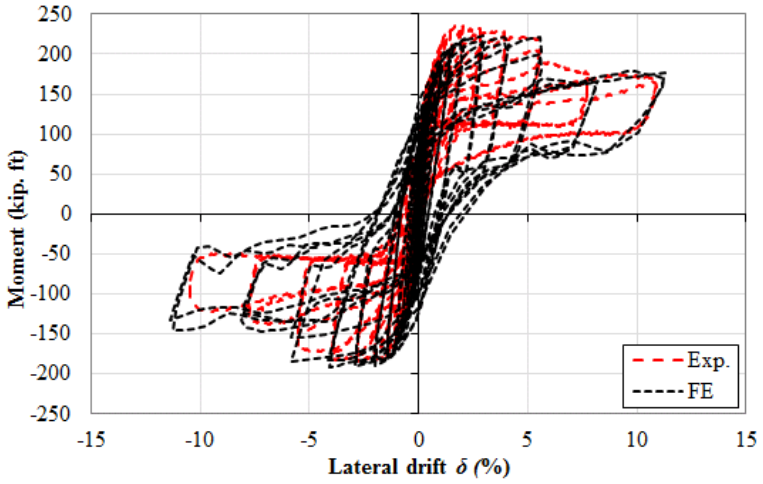

Figure 5. Moment vs. lateral drift hysteretic curve (experimental and FE)

Based on the experimental outcomes, column F4-24-E3(0.5)4 displayed narrow hysteretic loops. Furthermore, column F4-24-E3(0.5)4 displayed an approximately nonlinear elastic response (flag-shaped) due to sliding of the steel tube. The video recording and comprehensive finite element modeling as in Figure 6 showed that early local buckling in the case of column F4-24-E3(0.5)4 occurred near the footing-column interface joint which gradually extended downward leading to bond deterioration between the embedded steel tube and the surrounding concrete inside the footing. As shown in Figure 6 (a), the end section of the steel tube did not keep its circular shape. Thus, early initiation of the steel tube pull-out (slip) was observed at 2.65% lateral drift followed by flexural strength dropping as shown in Fig. 5.

The developed numerical model has effectively captured the hysteretic characteristics (strength and degradation) when the failure mode is dominated by inelastic deformation. Moreover, the model was able to capture the buckling failure mode of the thin-walled steel tube as well as the damage progression as is shown in Fig. 6 (b). The initiation and progression of the steel tube buckling were captured accurately on both sides of the column as observed in the video recording during the experimental test.

Figs. 7 and 8 show the FE effective plastic and the longitudinal strain of the steel tube at various lateral drift levels. These results were obtained from two elements on both sides of the loading directions at the interface between the column and the top level of the footing. As shown in Fig. 7, at a low lateral drift level (ranging from 1-1.5%) a slightly visible buckling deformation occurred in the steel tube and the plastic strain started moving above the non-zero value, as in Fig. 7(b). At moderate lateral drift 5%, inward steel tube local buckling was clearly observed on both sides and both plastic and longitudinal strain exceeded the yield strain. Beyond 5% drift, the longitudinal and plastic strain reached the ultimate (fracture) strain on the north side, as in Figs. 7(b) and 8(b). After that, the flexural strength degradation by 28% for the column was clearly observed at 7.5% lateral drift, as in Fig. 5. These behavior and results were relatively consistent with the test result.

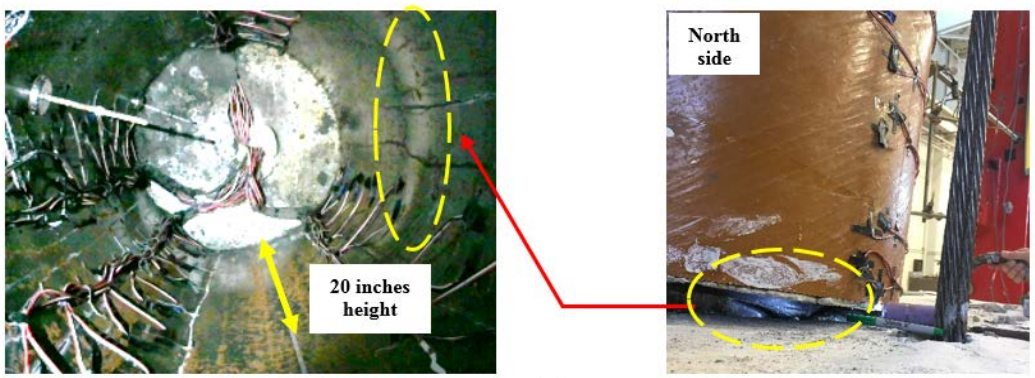

(a)

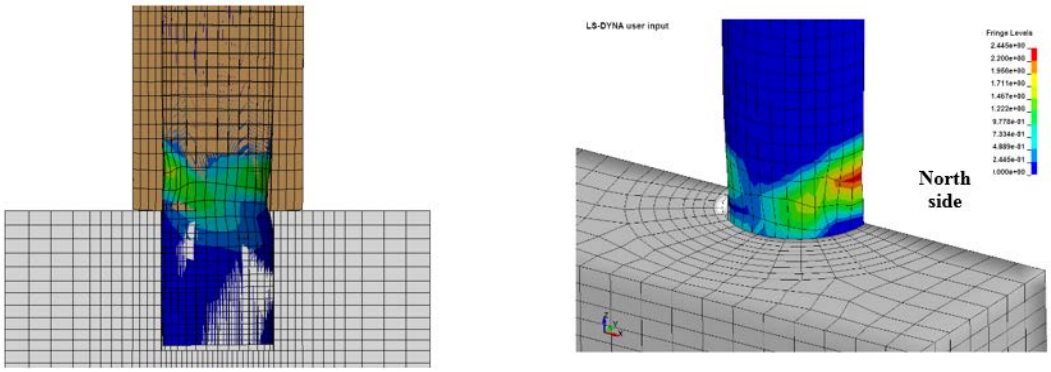

(b)

Figure 6. Thin-walled inner steel tube failure mode (a) experimental, (b) FE

It is worth mentioning that no tearing occurred in the steel tube after reaching the fracture strain, which matches accurately with the test observations. The reason is due to the steel tube slip as described above as well as the high D_i/t_s ratio of 254. Local buckling instabilities and localization in the steel tube are efficaciously captured in the numerical model based on the damage initiation and evolution model (DIEM). In general, the simulated model has effectively predicted the overall experimental cyclic behavior of HC-FCS columns and captured the steel tube strains at the interface joint.

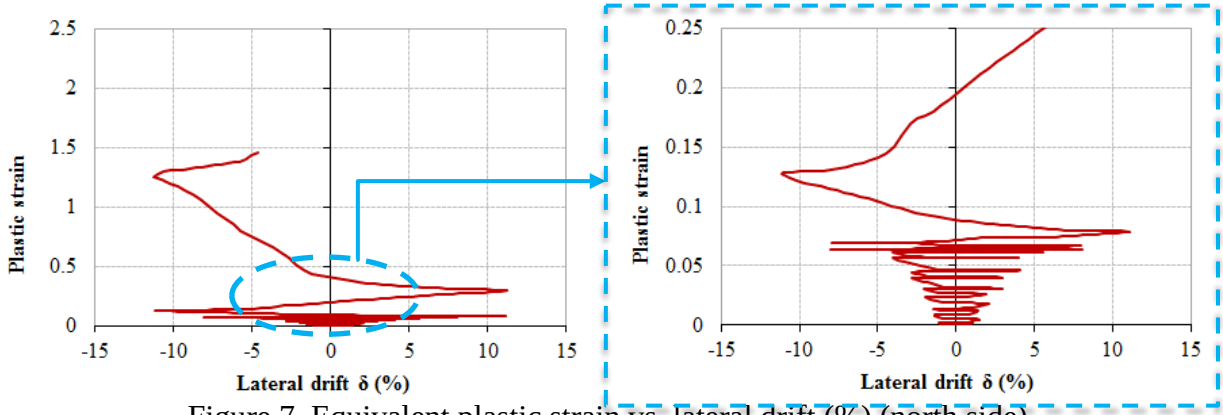

Figure 7. Equivalent plastic strain vs. lateral drift (%) (north side)

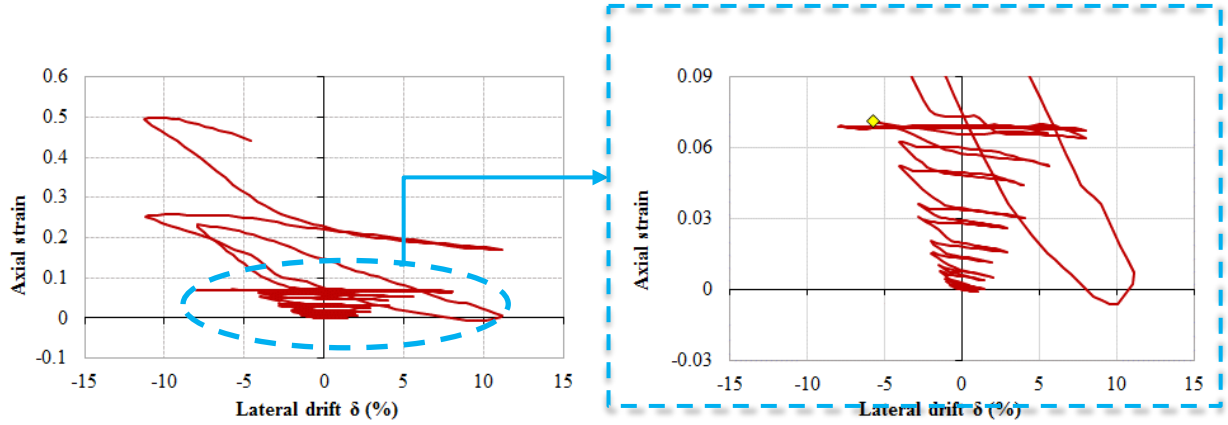

Figure 8. Longitudinal strain vs. lateral drift (%) (north side)

Conclusion

The proposed FEA model was developed using LS_DYNA software and was verified by experimental results performed in this study on large-scale HC_FCS columns having a thin-walled inner steel tube with a D_i/t_s ratio of 254. The FE model was used to investigate some important phenomena such as thin-walled steel tube cyclic local buckling and to determine where and when steel tube yielding and damage initiation occurs. The comparison and analysis of the proposed model to predict local damages, failure patterns, and hysteretic curves were in good agreement with the experimental results. The proposed FE 3D model can be used effectively to predict and capture the hysteretic curve, damage states, and the local buckling instabilities and localization as well as yielding of the inner steel tube.

References

1. Schrank, D., B. Eisele, and T. Lomax, *TTI's 2012 urban mobility report.* Texas A&M Transportation Institute. The Texas A&M University System, 2012: p. 4.
2. Schrank, D.L. and T.J. Lomax, *2009 urban mobility report*. 2009: Texas Transportation Institute, Texas A & M University.
3. Dawood, H., M. Elgawady, and J. Hewes, *Factors affecting the seismic behavior of segmental precast bridge columns.* Frontiers of Structural and Civil Engineering, 2014. **8**(4): p. 388-398.
4. Ozbakkaloglu, T. and B.L. Fanggi, *Axial compressive behavior of FRP-concrete-steel double-skin tubular columns made of normal-and high-strength concrete.* Journal of Composites for Construction, 2013.
5. Ozbakkaloglu, T. and Y. Idris, *Seismic behavior of FRP-high-strength concrete–steel double-skin tubular columns.* Journal of Structural Engineering, 2014.
6. Ozbakkaloglu, T. and B.A.L. Fanggi, *FRP–HSC–steel composite columns: Behavior under monotonic and cyclic axial compression.* Materials and Structures, 2013. **48**(4): p. 1075-1093.
7. Shakir-Khalil, H., *Composite columns of double-skinned shells.* Journal of Constructional Steel Research, 1991. **19**(2): p. 133-152.
8. Teng, J. and L. Lam, *Behavior and modeling of fiber reinforced polymer-confined concrete.* Journal of structural engineering, 2004. **130**(11): p. 1713-1723.

9. Ozbakkaloglu, T. and E. Akin, *Behavior of FRP-confined normal-and high-strength concrete under cyclic axial compression.* Journal of Composites for Construction, 2011. **16**(4): p. 451-463.
10. Abdelkarim, O.I. and M.A. ElGawady, *Behavior of hollow FRP–concrete–steel columns under static cyclic axial compressive loading.* Engineering Structures, 2016. **123**: p. 77-88.
11. Anumolu, S., O.I. Abdelkarim, and M.A. ElGawady, *Behavior of hollow-core steel-concrete-Steel Columns Subjected to Torsion Loading.* Journal of Bridge Engineering, 2016: p. 04016070.
12. Abdulazeez, Mohanad M., Omar I. Abdelkarim, Ahmed Gheni, Mohamed A. ElGawady, and Greg Sanders. *Effects of footing connections of precast hollow-core composite columns.* in Proc., Transportation Research Board (TRB) 96th Annual Meeting. No. 17-01256. 2017.
13. Abdelkarim, O.I., ElGawady, M. A., Gheni, A., Anumolu, S., and Abdulazeez, M., *Seismic performance of innovative hollow-core FRP–concrete–steel bridge columns.* Journal of Bridge Engineering, 2016: p. 04016120.
14. Abdelkarim, O.I. and M.A. ElGawady, *Analytical and finite-element modeling of FRP-concrete-steel double-skin tubular columns.* Journal of Bridge Engineering, 2014.
15. Youssf, O., et al., *Finite element modelling and dilation of FRP-confined concrete columns.* Engineering Structures, 2014. **79**: p. 70-85.
16. Ryu, D., et al., *Effects of tendon spacing on in-plane behavior of posttensioned masonry walls.* Journal of Structural Engineering, 2013. **140**(4): p. 04013096.
17. Malvar, L.J., et al., *A plasticity concrete material model for DYNA3D.* International Journal of Impact Engineering, 1997. **19**(9): p. 847-873.
18. Huang, Y. and S.A. Mahin. *Evaluation of steel structure deterioration with cyclic damaged plasticity*. in *The 14th World Conference on Earthquake Engineering, Beijing, China*. 2008.
19. Hallquist, J.O., *LS-DYNA3D theoretical manual*. 1994: Livermore software technology corporation Livermore, CA.
20. Imani, R., *Post-earthquake fire resistance of ductile concrete filled double-skin tube columns*. 2014: State University of New York at Buffalo.